

Measurement-induced topological entanglement transitions in symmetric random quantum circuits

Ali Lavasani, Yahya Alavirad, and Maissam Barkeshli

Department of Physics, Condensed Matter Theory Center,

University of Maryland, College Park, Maryland 20742, USA and

Joint Quantum Institute, University of Maryland, College Park, Maryland 20742, USA

We study a class of (1+1)D symmetric random quantum circuits with two competing types of measurements in addition to random unitary dynamics. The circuit exhibits a rich phase diagram involving robust symmetry-protected topological (SPT), trivial, and volume law entangled phases, where the transitions are hidden to expectation values of operators and can only be accessed through the entanglement entropy averaged over quantum trajectories. In the absence of unitary dynamics, we find a purely measurement-induced critical point with logarithmic scaling of the entanglement entropy, which we map exactly to two copies of a classical 2D percolation problem. We perform numerical simulations that indicate this transition is a tricritical point that splits into two critical lines in the presence of arbitrarily sparse unitary dynamics with an intervening volume law entangled phase. Our results show how measurements alone are sufficient to induce criticality and logarithmic entanglement scaling, and how arbitrarily sparse unitary dynamics can be sufficient to stabilize volume law entangled phases in the presence of rapid yet competing measurements.

I. INTRODUCTION

Generic unitary dynamics drive quantum many-body systems into highly entangled states characterized by volume-law scaling of subsystem entanglement entropies. When this dynamics is intercepted by rapid enough local measurements, individual quantum trajectories are expected to collapse into low entanglement states characterized by area-law scaling of subsystem entanglement entropies. Recently, it was discovered that, at least in a class of models, these two phases are separated by a scale-invariant “critical point” at a finite measurement rate [1–3]. Several aspects of this transition and its generalizations have been studied recently [4–18].

In the limit of infinitely rapid local measurements, the state of the system crucially depends on the choice of measurement basis. Assuming one measures only commuting single-qubit operators, the wave-function collapses into an unentangled trivial product-state. However, if one chooses to measure a set of *stabilizer* operators that stabilize a topological or a symmetry protected topological (SPT) wave-function, the resulting state, despite having area-law scaling of entanglement as well, would be *distinct* from the product state, in the sense that no (symmetry preserving) finite depth local unitary quantum circuit can transform the two states into each other [19, 20].

In this work, we consider the competition between these two types of measurements with each other as well as with the unitary dynamics. This raises the question of whether the notion of a topological phase is well-defined in random quantum circuits that include both unitary dynamics and local measurements and, if so, what are the properties of the associated phase transitions? To make progress in answering these questions, we consider a (1+1)D quantum circuit model comprised of three different elements: (a) Measurement of stabilizer operators that stabilize a $\mathbb{Z}_2 \times \mathbb{Z}_2$ SPT realized by the “cluster model” [21, 22]; (b) Single-qubit measurements in the computational basis (that commute with the $\mathbb{Z}_2 \times \mathbb{Z}_2$ symmetry). (c) Random, symmetry-allowed Clifford unitary gates (Clifford gates are considered to make classical simulation possible [23]). At each step of the circuit, one of these elements is selected at random with probability p_t , p_s , p_u respectively

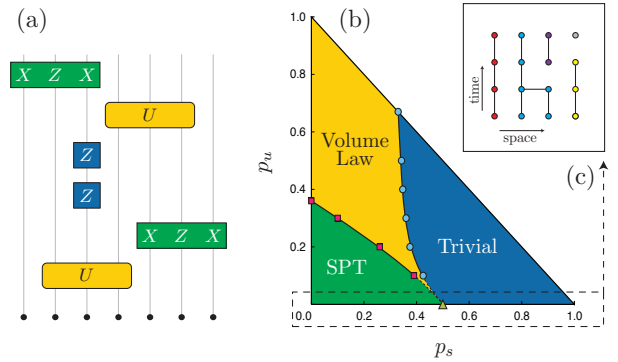


FIG. 1. (a) Schematic diagram of a typical quantum circuit. Yellow (light) boxes corresponds to a three qubit random Clifford unitary, blue and green boxes represent projective measurements. (b) The phase diagram describing the entanglement structure of the steady state. Red squares and blue circles are obtained from numerical simulations, while the rest of the phase boundaries are extrapolated. (c) Mapping the dynamics of the random circuit on the $p_u = 0$ axis to the 2D percolation on a square lattice.

($p_t + p_s + p_u = 1$) and applied at a random position in space. A typical snapshot of the circuit is shown in Fig. 1a.

We find that while expectation values of operators do not exhibit any transition, a suitably defined topological entanglement entropy, averaged over the quantum trajectories, does exhibit a rich phase diagram, shown in Fig. 1b. We find not only a stable SPT phase in an extended region of the phase diagram, but our results indicate a tricritical point, with logarithmic scaling of entanglement entropy, separating the volume law, trivial and SPT phases *in the absence of unitary dynamics* $p_u = 0$, i.e. when only measurements are present. The existence of this tricritical point implies that a volume-law phase can be stabilized by an infinitesimally small rate of unitary dynamics. This is remarkable since the existence of the volume law phase in the presence of arbitrarily small rates of measurements was already surprising [3, 12]; here we find

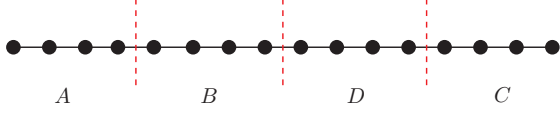


FIG. 2. The 1D chain cutting used to define the generalized topological entanglement entropy in Eq.(3)

that the volume law phase can be completely stable to arbitrarily high measurement rates as long as some arbitrarily small unitary dynamics is present.

Moreover, we find an *exact* analytical mapping that maps the case without unitary dynamics $p_u = 0$, including the tricritical point, to two copies of a (non-standard) classical 2D percolation problem. Away from the $p_u = 0$ line, we extensively study the phase transitions numerically throughout the phase diagram. We find that the correlation length critical exponent $\nu = 4/3$ and has the same value along the phase boundaries, equal to its value at the tricritical point (within the margin of error), which is in turn set by the corresponding value in the classical percolation problem. However, the coefficient of the logarithmic scaling of the entanglement entropy changes significantly along the phase boundaries, suggesting that the universality class changes along the phase boundaries.

II. THE MODEL AND ORDER PARAMETERS

We are interested in a family of (1+1)D random quantum circuits that realize quantum trajectories extrapolating between wave functions in an SPT phase, a trivial product state, and a volume-law entangled phase.

We take our SPT to be the $\mathbb{Z}_2 \times \mathbb{Z}_2$ symmetry protected phase realized by the cluster model defined on an open chain of N qubits (we take N even throughout) in (1+1)D [21, 22],

$$H_0 = - \sum_{i=2}^{N-1} X_{i-1} Z_i X_{i+1}, \quad (1)$$

where X_i and Z_i denote Pauli matrices acting on the i 'th qubit. Note that all terms commute with each other and therefore this model is exactly solvable. This model realizes a SPT phase [24, 25] protected by the $\mathbb{Z}_2 \times \mathbb{Z}_2$ symmetry generated by

$$G_1 = \prod_{i \text{ is even}} Z_i; \quad G_2 = \prod_{i \text{ is odd}} Z_i. \quad (2)$$

We say an eigenstate of H_0 is a symmetry invariant eigenstate if it is an eigenstate of all terms in H_0 as well as G_1 and G_2 . All symmetry invariant eigenstates within the same symmetry sector can be related to each other by a symmetry-preserving constant depth local unitary circuit.

On an open chain, a particular generalization of entanglement entropy [22, 26, 27] can be used as an order parameter for this SPT phase [28]. Consider dividing the system as

shown in Fig. 2. The generalized topological entanglement entropy S_{topo} is defined as

$$S_{\text{topo}} \equiv S_{AB} + S_{BC} - S_B - S_{ABC}. \quad (3)$$

S_{AB} stands for the von Neumann entanglement entropy of the region $A \cup B$ in the chain. Other terms are defined similarly. One can show that for all symmetry invariant eigenstates of H_0 , $S_{\text{topo}} = 2$.

To realize a wave function in this SPT phase, that is, a symmetry invariant eigenstate of H_0 , we can for example use a quantum circuit that starts with an arbitrary eigenstate of G_1 and G_2 and then proceed to measure all stabilizer operators $g_i \equiv X_{i-1} Z_i X_{i+1}$.

To realize wave functions in the trivial phase, we use a quantum circuit that measures all single qubit operators in the Z_i basis. The choice of the single qubit measurement basis Z_i is fixed by demanding all measurement operators commute with the symmetry generators G_1 and G_2 (see Appendix A for the case with symmetry violating measurements). All wave functions in the trivial phase have $S_{\text{topo}} = 0$.

To realize wave functions in the volume law phase, we use random Clifford unitary gates that are allowed by the symmetry. The simplest class of gates to consider would be two qubit nearest-neighbor random unitaries. However, due to the symmetry restrictions, this set is not effective in entangling the qubits. In particular, such gates always leave the $|0\rangle^{\otimes N}$ state untouched. Ergo, we work with three-qubit random unitary gates. Using such three-qubit random unitary gates we can easily drive the system into a volume law phase.

We are now in a position to construct our full quantum circuit model: We start with an arbitrary eigenstate of G_1 and G_2 (e.g. the $|0\rangle^{\otimes N}$ state). In each updating step we either: (a) apply a random 3-qubit Clifford unitary between qubits $i-1$, i and $i+1$ with probability p_u , for a random i drawn from $2, \dots, N-1$, (b) measure the single qubit operator Z_i with probability p_s , for a random i drawn from $1, \dots, N$, or (c) measure the stabilizer $g_i \equiv X_{i-1} Z_i X_{i+1}$ with probability $p_t = 1 - p_s - p_u$, for a random i drawn from $2, \dots, N-1$. A time step is defined as N consecutive updating steps. A typical example of such a circuit is shown in Fig. 1a.

In the limiting case $p_u = 1$ and $p_s = 0$, the random unitary circuit drives the system into a volume law phase, whereas for the other two limiting cases, i.e. $p_u = 0, p_s = 0$ and $p_u = 0, p_s = 1$, the system is in an area law phase, one with SPT order and the other without.

We detect the presence of the different phases in two distinct ways. First, at each time step we calculate S_{topo} , averaged over quantum trajectories, and run the circuit until a steady state value is obtained. In addition to S_{topo} , to detect the phase transition from the area to volume law phase we extensively use the order parameter introduced in Ref. [6]. To do so, first we run the circuit for time $2N$ to reach the steady state. Then, we entangle an ancilla qubit to the two qubits in the middle of the chain by measuring the following stabilizers,

$$Z_{N/2-1} Z_a, \quad Z_{N/2+1} Z_a, \quad X_{N/2-1} X_a X_{N/2+1}, \quad (4)$$

where X_a and Z_a act on the ancilla qubit. Note that all three stabilizers commute with the symmetry generators G_1 and

G_2 . Next, we let the circuit run for an extra $\mathcal{O}(N)$ time steps, and then measure the the entanglement entropy of the ancilla qubit. As shown in Ref. [6], if the system is in the area law phase, we expect the ancilla qubit to disentangle from the system in constant time, thus its entanglement entropy should be zero by the time we measure it. On the other hand, in a volume law phase, the time it takes for the circuit to disentangle the ancilla is exponentially large in system size and hence after $\mathcal{O}(N)$ time steps, the ancilla should still remain entangled with the system.

As we discuss in Section. IV, we find that the ancilla order parameter S_a appears to be unable to capture the SPT to trivial phase transition present at $p_u = 0$ and $p_s = 1/2$.

Finally, we note that the entanglement phase transitions we study cannot be detected using expectation values of operators. This is because the random quantum circuits studied here, viewed as a quantum channel, eventually transform the initial state of the system into the maximally mixed state allowed by the symmetry (see Appendix C for a proof and a bound on how fast this happens). Therefore, the steady state expectation value of *any* operator stays the same throughout the phase diagram and thus cannot serve as an order parameter.

III. MAPPING THE CASE WITHOUT UNITARY DYNAMICS $p_u = 0$ TO CLASSICAL PERCOLATION

Here we show how to map the entire $p_u = 0$ line in the random circuit presented above to two copies of a classical 2D percolation problem on a square lattice. This percolation model is non-standard, although our numerical results indicate that it has the same critical properties as the standard classical percolation model on the square lattice. There is a distinct but closely related random quantum circuit that we define in Appendix H which does map directly to (two copies of) standard classical percolation.

Let us divide the operators measured by the random circuit into two sets. One set, which we call the odd site operators, is comprised of single qubit operators Z_i for odd i alongside the stabilizers g_j which *end* on the odd sites, i.e. for even j . The even site operators are defined analogously. Note that each member of one set commutes with all elements of the other set.

Let us focus on the measurements of odd site operators. Consider the $N/2 \times M$ square lattice as shown in Fig. 1c, where M is the total number of updating steps in the circuit. We call this lattice the odd sites' percolation lattice. The $N/2$ vertices on each row corresponds to the odd sites of the system and we label them accordingly. The vertical (horizontal) links ending (residing) on the m 'th row are related to the Z_i (g_j) measurements in the m 'th step of the circuit in the following way: if Z_i is *not* measured at updating step m , we draw a vertical link between the $(i, m - 1)$ and (i, m) vertices. Also if the stabilizer g_j is measured at step m , we draw a horizontal link between the $(j - 1, m)$ and $(j + 1, m)$ vertices. At the end, we assign a unique color to each connected cluster of vertices. We construct the even sites' percolation lattice anal-

ogously. The randomness of the quantum circuit translates into random connections in the percolation lattices; the probability distributions for the links in the percolation lattice are detailed in Appendix D. Note that since at each updating step we only measure one operator, the corresponding percolation lattice has at most one vertical link missing in each row, and at most one horizontal link present in each row.

The entanglement entropy of the system at step M can be extracted from the colors of the vertices on the last row of the two aforementioned percolation lattices. As the following proposition makes precise, qubits of the same color make up their own SPT state:

Proposition 1. Group the qubits based on their color on the last row of the percolation lattice. Let $A^j = \{q_i\}_{i=1}^n$ denote the ordered set of qubit indices corresponding to j 'th color; that is, the q_i label a set of qubits all with the same color at step M . Then, up to a minus sign, the operators that stabilize the state of the system at step M are of the following form,

$$\prod_{i=1}^n Z_{q_i} \quad \text{and} \quad g_{q_i, q_{i+1}} \quad \text{for } i = 1, 2, \dots, n-1, \quad (5)$$

where $g_{q_i, q_{i+1}}$ is defined as

$$g_{i,j} = X_i \left[\prod_{k=0}^{\frac{j-i}{2}-1} Z_{i+2k+1} \right] X_j. \quad (6)$$

By considering similarly defined stabilizer operators for all different colors (A^j 's with different j), we get a complete set of stabilizers that specify the state of the system.

The ground state of the SPT Hamiltonian (1) corresponds to the case where all odd sites have one color while all even sites have another color. On the other hand, the product state wave function corresponds to the case where each site has its own unique color. The proof of Proposition 1 is left for Appendix G.

As shown in Lemma 1 in Appendix B, the minus sign ambiguity in Proposition 1 has no bearing on the entanglement spectrum of the system's state. Thus the percolation lattices exactly determine the (von Neumann or R nyi) entanglement entropy for any subset of qubits.

IV. NUMERICAL RESULTS

We start by briefly reviewing the quantities we numerically calculate to obtain the phase diagram and to characterize the critical phase boundaries.

A signature of criticality in (1+1)D systems is the logarithmic scaling of the entanglement entropy. Thus, we calculate the entanglement entropy at the t th time step (which corresponds to tN updating steps), $S(x, L; t)$ of a subsystem of length x for a system of total length $L = N$, averaged over all of the quantum trajectories of the circuit.

In the large time limit, this averaged entanglement entropy saturates to a logarithmic form at the phase transitions as in

(1+1)D CFTs [29]:

$$S(x, L) = a_x \log\left(\frac{L}{\pi} \sin \frac{\pi x}{L}\right) + b. \quad (7)$$

We can also characterize the entanglement growth with time. At criticality, for timescales much smaller than the saturation time we have,

$$S(x, L; t) = a_t \log(t) + b'. \quad (8)$$

Note that as opposed to unitary CFTs the coefficient of the logarithmic scaling a_x is not given by the central charge of any underlying CFT. In the context of the area law to volume law transition, Ref. [30] provides an appealing interpretation of a_x and a_t as universal quantities given by the scaling dimension of certain “boundary condition changing” operators. b and b' are non-universal constants

Throughout the phase boundaries, within the margin of error, we find $a_x = a_t$, which is consistent with a dynamical exponent $z = 1$, as the entanglement growth rate is similar along time and space directions.

We can use the averaged topological entanglement entropy, S_{topo} as the order parameter to distinguish the three different phases: S_{topo} would be extensive in the volume law phase, while in the thermodynamic limit it should converge to values 2 and 0 in the topological and trivial phases respectively. Let $S_{\text{topo}}(p, L)$ denote the steady state value of S_{topo} when some tuning parameter (e.g. single qubit measurement probability) is p and system size is L . On general grounds, we expect the following scaling form in the vicinity of the critical point,

$$S_{\text{topo}}(p, L) = F((p - p_c)L^{1/\nu}), \quad (9)$$

where $F(x)$ is some unknown function, p_c is the critical value of tuning parameter p , and ν is the correlation length critical exponent, $\xi \propto |p - p_c|^{-\nu}$.

As explained in Sec. II, the entanglement entropy S_a of an ancilla qubit can also be used as the order parameter to distinguish the volume law phase from the other two area law phases. Assuming the dynamical exponent $z = 1$, for the ancilla entropy S_a we have [6],

$$S_a(p, L, t) = G((p - p_c)L^{1/\nu}, t/L), \quad (10)$$

where $G(x)$ is some unknown function.

We now present our numerical results. We study system sizes up to 512 qubits and average over 10^5 random quantum trajectories. We start with the $|0\rangle^{\otimes N}$ state and let the circuit run for $2N$ time steps for the system to reach the steady state. We have explicitly verified that saturation is reached before $t = 2N$. After entangling the ancilla qubit, we simulate the system for an additional $\mathcal{O}(N)$ time steps to calculate S_a (as explained above).

Fig. 3 shows numerical results along the $p_u = 0$ line. Fig. 3a shows the steady state value of S_{topo} versus p_s for different system sizes. As is evident from the diagram, there is a clear continuous phase transition at $p_c = 1/2$ in the thermodynamic limit. A simple argument based on duality shows that

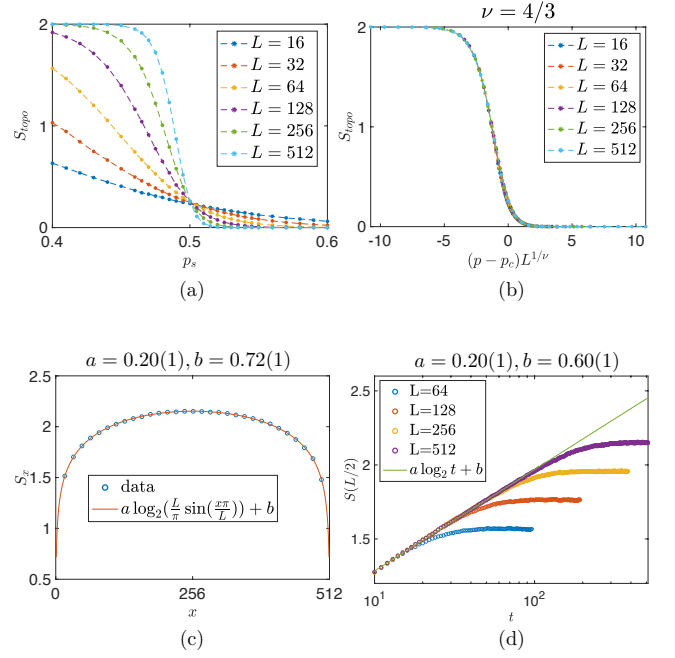


FIG. 3. (a) Topological entanglement entropy S_{topo} near the tricritical point (at $p_u = 0$) versus single qubit measurement probability. (b) Scaling collapse of the data in (a). (c) The entanglement entropy of the $[0, x]$ segment of the chain, $S(x, L)$, at late times for $p = p_c$ and $L = 512$. (d) The entanglement entropy of the half-chain versus time for $p_s = p_c$. All entropies are in units of $\log 2$.

if there is a continuous phase transition between the trivial and topological phase, it has to be at $p_s = 1/2$. This duality argument is provided in Appendix E. Interestingly we find that S_a seems to be unable to capture the area-law to area-law phase transition at $p_u = 0$, at least for numerically accessible systems sizes. From collapsing the data near the critical point $p_c = 1/2$, we find $\nu = 4/3$ results in a near perfect collapse (see Fig. 3b).

Fig. 3c shows the steady state value of entanglement entropy $S(x)$ of the subregion $[1, x]$ at the critical point $p_u = 0$ and $p_s = 1/2$, for $L = 512$. As shown, the entanglement entropy fits the CFT form of Eq. (7) with $a_x = 0.20(1)$.

Fig. 3d shows the entanglement entropy of the half chain versus time at $p = p_c$ for different chain sizes. The entanglement entropy grows logarithmically with time, until the finite size effects show up. By comparing the corresponding fitted analytical expressions we find $a_t = a_x = 0.20(1)$.

We note that the values of ν , z , a_x , and a_t at the $p_u = 0$, $p_s = 1/2$ transition agree with the values of our other random measurement-based quantum circuit model presented in Appendix H, which in turn maps to (two copies of) the standard classical link percolation problem on the square lattice. Our results are thus consistent with the $p_u = 0$, $p_s = 1/2$ transition studied in Fig. 3 being governed by (two copies of) the standard classical percolation fixed point.

We now proceed to the case with unitary dynamics $p_u \neq 0$. Fig. 4 shows S_{topo} and S_a versus p_s for the fixed value of $p_u = 0.3$. For $p_s = 0$, the system is in the topological

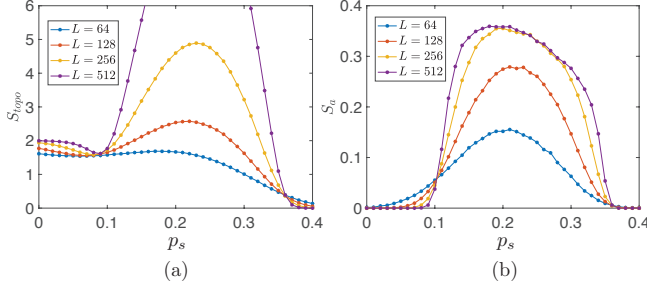


FIG. 4. (a) S_{topo} versus p_s for fixed $p_u = 0.3$. (b) The ancilla entropy S_a measured N time steps after it was entangled, versus p_s for fixed $p_u = 0.3$. In both plots, the first crossing corresponds to the phase transition from the SPT phase into the volume law phase while the second crossing corresponds to the phase transition from the volume law phase to the trivial phase. The critical points are marked on the phase diagram in Fig. 1b as well.

phase as can be seen from Fig. 4a. By increasing p_s , the entropies exhibit a continuous phase transition to the volume law phase at first and then another continuous phase transition to the trivial phase.

By using analogous plots for different values of p_u , we can determine the 2D phase diagram in the (p_s, p_u) space. The result is illustrated in Fig. 1b. Note that since the probability of measuring a stabilizer is $1 - p_u - p_s$, the phase diagram is restricted to the region $p_u + p_s \leq 1$. The data points on the plot have been extracted using numerical simulations and then the schematic phase diagram is drawn based on them. For more detailed results used in obtaining the phase diagram see Appendix I.

The SPT/volume law phase boundary intersects the p_u axis at $p_u = 0.355(5)$ and the volume law/trivial phase boundary ends at $p_u = 0.665(5)$ on the $p_u + p_s = 1$ line. Our numerical simulations demonstrate that the volume law phase still exists for p_u as low as 0.1. Unfortunately, clearly detecting the SPT to volume law transition requires increasingly large system sizes as p_u is lowered. Therefore, we extrapolate the phase diagram for smaller values of p_u . By following the trend of the data points, it appears that the volume law phase survives all the way down to $p_u = 0$, hence suggesting that the critical point at $p_s = 0.5$ and $p_u = 0$ is actually a tricritical point. This in turn means that at $p_s = 1/2$, arbitrarily sparse random Clifford gates in the quantum circuit can still drive the system into the volume law phase.

By using the scaling form in Eq. (9) and collapsing the data, we can extract the correlation length critical exponent ν along the phase boundaries. We found that $\nu = 4/3$, within the margin of error, everywhere along the phase boundaries (see Appendix I for the corresponding plots and numerical values). However the coefficient of the logarithmic scaling of entanglement entropy $a_x = a_t$ changes significantly along the phase boundaries, with different values at each data point we have studied, suggesting that they change continuously along the phase boundaries. If these are indeed universal quantities then this suggests different universality classes despite having the same correlation length exponent, thus indicating that the vol-

ume to area law critical lines are related to two copies of the classical percolation fixed point by marginal deformations.

V. DISCUSSION

We have demonstrated the existence and stability of a generalized SPT phase in a class of random quantum circuits. We further find evidence for a tricritical point separating the SPT, trivial product state, and volume-law entangled phases, which occurs in the absence of unitary dynamics $p_u = 0$. To our knowledge, this is first example of measurement-induced criticality where unitary dynamics is not necessary. Moreover, the existence of the volume law phase appears stable for arbitrarily sparse unitary dynamics, since the competition between the different types of measurements completely frustrates the presence of an area law phase. Remarkably, the tricritical point can be mapped exactly to two copies of a classical percolation problem, which suggests that the area to volume law transitions may be thought of as a marginal deformation of two copies of the 2D classical percolation fixed point.

The transitions we have studied can be detected by examining entanglement entropies averaged over the space of quantum trajectories, while simple expectation values of operators never see any sign of a transition. It is thus a fundamental question to understand to what extent these transitions, when generalized beyond the random Clifford circuits we have studied, can be accessed experimentally, even using a quantum computer, in time that is polynomial in the number of qubits. While there is a proposal to access the volume law to area law transitions in polynomial time using ancilla qubits [6], we have not been able to use this ancilla order parameter to detect the area law to area law transition in our paper.

Entanglement phase transitions involving topological or SPT phases seem to be closely related to quantum error correction. In particular, the rapid stabilizer measurements are reminiscent of syndrome measurements in active error correction schemes. Moreover, random single qubit measurements can be viewed as faulty syndrome measurements or qubit decoherence, while unitary dynamics models the random noise affecting the qubits. In this context, “entanglement phase transitions” could be related to “error-thresholds” beyond which the long range entanglement structure of the code space, which is responsible for the topological protection of the encoded information, is entirely lost, hence rendering recovery of logical information impossible. Within this framework, our results might have natural applications to error correcting quantum codes. Note that this is a different analogy to quantum error correction than the one presented in Ref. [5, 8], where the volume law phase is considered to be a quantum error correcting code.

VI. ACKNOWLEDGEMENTS

We are grateful to Mohammad Hafezi and Hossein Dehghani for their valuable insights. The authors acknowledge the University of Maryland supercomputing resources

(<http://hpcc.umd.edu>) made available for conducting the research reported in this paper. A.L and M.B are supported by NSF CAREER (DMR- 1753240), Alfred P. Sloan Research

Fellowship, and JQI- PFC-UMD. Y.A is supported by National Science Foundation NSF DMR1555135 and JQI-NSF-PFC.

-
- [1] B. Skinner, J. Ruhman, and A. Nahum, *Physical Review X* **9**, 031009 (2019).
 - [2] Y. Li, X. Chen, and M. P. Fisher, *Physical Review B* **98**, 205136 (2018).
 - [3] A. Chan, R. M. Nandkishore, M. Pretko, and G. Smith, *Phys. Rev. B* **99**, 224307 (2019).
 - [4] Y. Li, X. Chen, and M. P. Fisher, *Physical Review B* **100**, 134306 (2019).
 - [5] M. J. Gullans and D. A. Huse, (2019), [arXiv:1905.05195](https://arxiv.org/abs/1905.05195).
 - [6] M. J. Gullans and D. A. Huse, [arXiv preprint arXiv:1910.00020](https://arxiv.org/abs/1910.00020) (2019).
 - [7] R. Vasseur, A. C. Potter, Y.-Z. You, and A. W. W. Ludwig, *Phys. Rev. B* **100**, 134203 (2019).
 - [8] S. Choi, Y. Bao, X.-L. Qi, and E. Altman, (2019), [arXiv:1903.05124](https://arxiv.org/abs/1903.05124).
 - [9] M. Szyniszewski, A. Romito, and H. Schomerus, *Phys. Rev. B* **100**, 064204 (2019).
 - [10] Q. Tang and W. Zhu, *Phys. Rev. Research* **2**, 013022 (2020).
 - [11] C.-M. Jian, Y.-Z. You, R. Vasseur, and A. W. W. Ludwig, *Phys. Rev. B* **101**, 104302 (2020).
 - [12] X. Cao, A. Tilloy, and A. D. Luca, *SciPost Phys.* **7**, 24 (2019).
 - [13] J. Lopez-Piqueres, B. Ware, and R. Vasseur, (2020), [arXiv:2003.01138](https://arxiv.org/abs/2003.01138).
 - [14] Y. Bao, S. Choi, and E. Altman, *Phys. Rev. B* **101**, 104301 (2020).
 - [15] L. Piroli, C. Sünderhauf, and X.-L. Qi, (2020), [arXiv:2002.09236](https://arxiv.org/abs/2002.09236).
 - [16] A. Zabalo, M. J. Gullans, J. H. Wilson, S. Gopalakrishnan, D. A. Huse, and J. H. Pixley, *Phys. Rev. B* **101**, 060301 (2020).
 - [17] D. Rossini and E. Vicari, (2020), [arXiv:2001.11501](https://arxiv.org/abs/2001.11501).
 - [18] R. Fan, S. Vijay, A. Vishwanath, and Y.-Z. You, (2020), [arXiv:2002.12385](https://arxiv.org/abs/2002.12385).
 - [19] M. B. Hastings, *Phys. Rev. Lett.* **107**, 210501 (2011).
 - [20] X. Chen, Z.-C. Gu, Z.-X. Liu, and X.-G. Wen, *Physical Review B* **87**, 155114 (2013).
 - [21] R. Raussendorf and H. J. Briegel, *Physical Review Letters* **86**, 5188 (2001).
 - [22] B. Zeng, X. Chen, D.-L. Zhou, and X.-G. Wen, *Quantum information meets quantum matter* (Springer, 2019).
 - [23] D. Gottesman, *Ph.D. thesis* (1997), [10.7907/rzr7-dt72](https://arxiv.org/abs/10.7907/rzr7-dt72).
 - [24] W. Son, L. Amico, R. Fazio, A. Hamma, S. Pascazio, and V. Vedral, *EPL (Europhysics Letters)* **95**, 50001 (2011).
 - [25] L. Tsui, Y.-T. Huang, H.-C. Jiang, and D.-H. Lee, *Nuclear Physics B* **919**, 470 (2017).
 - [26] B. Zeng and X.-G. Wen, *Physical Review B* **91**, 125121 (2015).
 - [27] B. Zeng and D.-L. Zhou, *EPL (Europhysics Letters)* **113**, 56001 (2016).
 - [28] On a closed chain, based on the percolation mapping, we expect a similar but perhaps more complicated entanglement based order parameter to exist.
 - [29] P. Calabrese and J. Cardy, *Journal of Physics A: Mathematical and Theoretical* **42**, 504005 (2009).
 - [30] Y. Li, X. Chen, A. W. W. Ludwig, and M. P. A. Fisher, (2020), [arXiv:2003.12721](https://arxiv.org/abs/2003.12721).
 - [31] D. Fattal, T. S. Cubitt, Y. Yamamoto, S. Bravyi, and I. L. Chuang, [arXiv preprint quant-ph/0406168](https://arxiv.org/abs/quant-ph/0406168) (2004).
 - [32] A. Nahum, J. Ruhman, S. Vijay, and J. Haah, *Physical Review X* **7**, 031016 (2017).
 - [33] D. Gottesman, [arXiv preprint quant-ph/9807006](https://arxiv.org/abs/quant-ph/9807006) (1998).
 - [34] M. A. Nielsen and I. Chuang, “Quantum computation and quantum information,” (2002).

Appendix A: Circuits which do not respect the symmetry

To verify that the stability of the SPT phase in the circuit model of Section II depends on the circuit respecting the symmetry, we consider the same circuit model at $p_u = 0$ but with Z_i measurements replaced by X_i measurements. Fig. 5 shows the topological entanglement entropy in the steady state versus p_s for the aforementioned modified circuit. As expected, any infinitesimal p_s will destroy the topological phase in the thermodynamic limit.

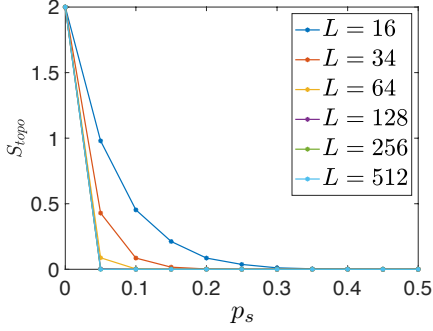


FIG. 5. S_{topo} versus p_s . The single qubit measurements are in the X_i basis rather than the Z_i basis.

Appendix B: Entanglement entropy in stabilizer formalism

A stabilizer state $|\psi\rangle$ over N qubits is specified by a set $\mathcal{S} = \{s_1, \dots, s_N\}$ of N independent, mutually commuting Pauli strings operators s_i , such that

$$s_i |\psi\rangle = |\psi\rangle. \quad (\text{B1})$$

Clearly, there are many equivalent choices of \mathcal{S} that result in the same stabilizer state $|\psi\rangle$. However, given a stabilizer set \mathcal{S} , the elements s_i generate an abelian group $\mathcal{G}_\psi = \langle s_1, s_2, \dots, s_N \rangle$ under multiplication, which is determined uniquely by the stabilizer state $|\psi\rangle$.

The density matrix of the system in the stabilizer state $|\psi\rangle$ can be written as [31]

$$\rho = |\psi\rangle\langle\psi| = \frac{1}{2^N} \sum_{g \in \mathcal{G}_\psi} g. \quad (\text{B2})$$

Given a bipartition of the qubits into two sets A and B , the reduced density matrix of ρ over A can be obtained by tracing Eq. (B2) over B , which yields

$$\rho_A = \frac{1}{2^{n_A}} \sum_{g \in \mathcal{G}_{A,\psi}} g, \quad (\text{B3})$$

where n_A is the number of qubits in A and $\mathcal{G}_{A,\psi} \subseteq \mathcal{G}_\psi$ is the subgroup of the stabilizers which are entirely contained in A , i.e. they act as identity on the qubits outside A . The von Neumann entanglement entropy of ρ_A is given by

$$S_A(|\psi\rangle) = n_A - \log_2 |\mathcal{G}_{A,\psi}|, \quad (\text{B4})$$

where $|\mathcal{G}|$ stands for the number of elements in group \mathcal{G} . Moreover, $R_\alpha(\rho_A)$, the Renyi entropy of order α , is actually independent of α and is equal to von Neumann entanglement entropy.

Let $|\psi\rangle$ be a stabilizer state specified by the stabilizer set $\mathcal{S} = \{s_1, s_2, \dots, s_N\}$. Consider a closely related stabilizer state $|\psi'\rangle$ which is specified by the stabilizer set $\mathcal{S}' = \{(-1)^{n_1} s_1, (-1)^{n_2} s_2, \dots, (-1)^{n_N} s_N\}$ where each n_i is either 0 or 1. The following Lemma shows that $|\psi\rangle$ and $|\psi'\rangle$ are indistinguishable as far as the entanglement entropy is concerned.

Lemma 1. For $|\psi\rangle$ and $|\psi'\rangle$ defined as above and for any subset A of the qubits,

$$S_A(|\psi\rangle) = S_A(|\psi'\rangle). \quad (\text{B5})$$

Proof. Let \mathcal{G}_ψ and $\mathcal{G}_{\psi'}$ denote the stabilizer groups associated with $|\psi\rangle$ and $|\psi'\rangle$ respectively. Consider the group homomorphism h between \mathcal{G}_ψ and $\mathcal{G}_{\psi'}$ defined by its action on the generators of \mathcal{G}_ψ as

$$\begin{aligned} h : \mathcal{G}_\psi &\longrightarrow \mathcal{G}_{\psi'} \\ h(s_i) &= (-1)^{n_i} s_i. \end{aligned}$$

Since h maps a generator set to another, it is bijective. Moreover, it is straightforward to verify that for any subset A of qubits, h maps $\mathcal{G}_{A,\psi}$ to $\mathcal{G}_{A,\psi'}$. The Lemma's claim then follows immediately from Eq. (B4). \square

Given a stabilizer state $|\psi\rangle$, one has the freedom to choose any N independent elements from \mathcal{G}_ψ to form the stabilizer set \mathcal{S} . We can use this gauge freedom to impose certain conditions on the elements of \mathcal{S} .

Define the left (right) endpoint of a stabilizer s to be the first (last) site on which s acts non-trivially. Given a set of stabilizers \mathcal{S} , let $\rho_l(i)$ denote the number of stabilizers whose left endpoint resides on site i and define $\rho_r(i)$ similarly with regard to the right end points. As is shown in Ref. [32], one can always choose \mathcal{S} such that

1. For all sites we have $\rho_r(i) + \rho_l(i) = 2$.
2. If $\rho_l(i) = 2$ (or $\rho_r(i) = 2$) for a site i , the two corresponding stabilizers have a different Pauli operator at i .

Such a stabilizer set \mathcal{S} is said to be in the clipped gauge [4]. The utility of the clipped gauge is that the entanglement entropy has a simple form in this gauge. In particular, if the stabilizer set \mathcal{S} is in the clipped gauge, the entanglement entropy of a contiguous region A equals to half the number of stabilizers in \mathcal{S} which have one endpoint in A and another in its complement [4].

Appendix C: Steady state density matrix

Let \mathcal{Q} denote a specific realization of the quantum circuit laid out in Section II. If we fix the initial state to be $|0\rangle^{\otimes N}$ and

run the same circuit many times, due to the randomness in the measurement outcomes, the final state of the system could be different each time. Instead of considering quantum trajectories, we can calculate the expectation value of operators over different runs by viewing the measurements in \mathcal{Q} as quantum channels. Accordingly, the entire circuit can be described as a quantum channel $\mathcal{E}_{\mathcal{Q}}$, which transforms the initial pure density matrix $\rho_0 = (|0\rangle\langle 0|)^{\otimes N}$ to a mixed final density matrix $\rho_* = \mathcal{E}_{\mathcal{Q}}(\rho_0)$.

ρ_* can be used to compute the expectation values of measurements which are averaged over many runs of the circuit without post-selection on the measurement outcomes. In particular, if we run the circuit \mathcal{Q} many times, measure a fixed operator O each time and average the result over a large number of runs, the value we get would be

$$\bar{O} = \text{tr}(O\rho_*). \quad (\text{C1})$$

Here we show that with probability one, ρ_* is actually independent of the underlying circuit. In other words, if \mathcal{Q} is any fixed quantum circuit chosen with the distribution associated with probabilities $0 < p_s, p_t < 1$ and $p_u < 1$, the final density matrix of the system is always given by

$$\rho_* = \mathcal{E}_{\mathcal{Q}}(\rho_0) = \frac{1}{2^{N-2}} \Pi_{G_1,+} \Pi_{G_2,+} \quad (\text{C2})$$

where $\Pi_{G_i,+}$ is the projection operator on the $G_i = 1$ subspace. Note that, not only does ρ_* not depend on the specific realization \mathcal{Q} , but it is also independent of p_s and p_u , which means that as far as the expectation value of operators is concerned, the entire phase space looks the same. Moreover, we show that the time it takes for the density matrix to reach the steady state is constant for $p_u = 0$ while it is at most $\mathcal{O}(N)$ for $p_u \neq 0$.

For a general Pauli string operator S , the quantum channel corresponding to its measurement is given by

$$\mathcal{E}_S(\rho) = \Pi_{S,+} \rho \Pi_{S,+} + \Pi_{S,-} \rho \Pi_{S,-} \quad (\text{C3})$$

where Π_{\pm} denote the projectors onto $S = \pm 1$ subspaces, i.e.

$$\Pi_{S,\pm} = \frac{1}{2}(\mathbb{1} \pm S). \quad (\text{C4})$$

By using the explicit form of the projectors $\Pi_{S,\pm}$, Eq. (C3) can be written as

$$\mathcal{E}_S(\rho) = \frac{1}{2}(\rho + S \rho S). \quad (\text{C5})$$

Consider a mixed stabilizer state ρ

$$\rho(\mathcal{G}) = \frac{1}{2^N} \sum_{g \in \mathcal{G}} g, \quad (\text{C6})$$

for a Pauli group $\mathcal{G} = \langle e_1, \dots, e_n \rangle$ with $n \leq N$ independent generators. According to Eq. (C5), under the measurement of

a Pauli string S , we have

$$\mathcal{E}_S(\rho) = \frac{1}{2^{N+1}} \left(\sum_{g \in \mathcal{G}} g + \sum_{g \in \mathcal{G}} S g S \right) \quad (\text{C7})$$

$$= \frac{1}{2^N} \sum_{g \in C_{\mathcal{G}}(S)} g \quad (\text{C8})$$

$$= \rho(C_{\mathcal{G}}(S)). \quad (\text{C9})$$

Here $C_{\mathcal{G}}(S)$ is the centralizer of S in \mathcal{G} . If S commutes with all elements in \mathcal{G} , clearly $C_{\mathcal{G}}(S) = \mathcal{G}$. Otherwise, without loss of generality, we can assume S commutes with all generators of \mathcal{G} except one of them, say e_n . Thus $C_{\mathcal{G}}(S) = \langle e_1, \dots, e_{n-1} \rangle$.

The above analysis shows that for a mixed stabilizer state, whenever a Pauli string is measured, it either leaves the density matrix untouched or takes it to another mixed stabilizer state with one less generator, depending on whether the measured Pauli string commutes with the corresponding Pauli group or not.

In our case, the initial state of the system is given by

$$\rho(\mathcal{G}_0) = \frac{1}{2^N} \sum_{g \in \mathcal{G}_0} g, \quad \mathcal{G}_0 = \langle G_1, G_2, Z_2, \dots, Z_{N-1} \rangle. \quad (\text{C10})$$

Let us first consider the $p_u = 0$ case. Based on the discussion above, it is clear that Z_i measurements never change ρ and thus can be ignored for our purpose. Each time a stabilizer g_i is measured, $\rho(\mathcal{G})$ is transformed to $\rho(C_{\mathcal{G}}(g_i))$. Note that in general we have

$$C_{C_{\mathcal{G}}(S_1)}(S_2) = C_{\mathcal{G}}(\{S_1, S_2\}). \quad (\text{C11})$$

Thus after all stabilizers g_i have been measured at least once, the density matrix of the system would be given by:

$$\begin{aligned} \rho(C_{\mathcal{G}_0}(\{g_2, \dots, g_{N-1}\})) &= \rho(\langle G_1, G_2 \rangle) \\ &= \frac{1}{2^{N-2}} \Pi_{G_1,+} \Pi_{G_2,+} = \rho_*. \end{aligned} \quad (\text{C12})$$

Let m_j denote the updating step at which g_j is measured for the first time. It is easy to show that $\mathbb{E}[m_j] = (N-2)/p_t$, where $\mathbb{E}[X]$ denotes the expectation value of X . Therefore, the average time it takes for the system to reach the steady state ρ_* would be

$$\tau_* = \frac{1}{N} \mathbb{E}[\max_j(m_j)] = \frac{1}{N} \max_j(\mathbb{E}[m_j]) = \mathcal{O}(1), \quad (\text{C13})$$

where the pre-factor $1/N$ is there to convert updating steps to time steps.

Now consider the $p_u \neq 0$ case. Again, we start by the same initial density matrix given by Eq. (C10). Each time a measurement is performed, either Z_i or g_i , the Pauli group associated with the density matrix of the system either remains the same or shrinks to one of its subgroups with one less generator, as was explained above. On the other hand, whenever a Clifford unitary U is applied, it just transform $\rho(\mathcal{G})$ to

$\rho(U^\dagger \mathcal{G} U)$ with the same number of generators. Now, note that any Pauli group that commutes with every element in the set $\mathcal{M} = \{Z_i\}_{i=1}^N \cup \{g_i\}_{i=2}^{N-1}$ should be a subgroup of $\langle G_1, G_2 \rangle$ (or the ones which are obtained by substituting G_i with $-G_i$). Therefore, for any Pauli group \mathcal{G} with more than two generators, there is at least one element of \mathcal{M} that does not commute with \mathcal{G} . Ergo, at each updating step with probability of at least $\min(p_s/N, p_t/(N-2))$, the Pauli group associated with the density matrix would shrink to a subgroup with one less generator, until only two generators G_1 and G_2 remain. Thus, on average, at most it takes $\mathcal{O}(N)$ updating steps until a stabilizer is measured which decreases the number of generators by one. Since we start with N generators, the average time it takes to reach the steady state with only G_1 and G_2 as generators, i.e. ρ_* , would be:

$$\tau_* \leq \frac{1}{N}(N-2)\mathcal{O}(N) = \mathcal{O}(N). \quad (\text{C14})$$

Appendix D: Mapping the random circuit model to an unconventional percolation model

Here we add some additional details regarding the the unconventional classical percolation model that corresponds to the random quantum circuit studied in the manuscript.

We focus on one of the two percolation lattices, say the odd sites' percolation lattice. Consider the $N/2 \times M$ square lattice of vertices. The connections on the m 'th row and the connections between the rows m and $m-1$, which are related to the measurement at step m , are determined as follows:

- With probability $\frac{1}{2}$ all vertical links between rows $m-1$ and m are connected and all horizontal links on the m 'th row are broken. This corresponds to the case where at step m , one of the even site operators is measured.
- With probability $\frac{1}{2}p_s$ a random vertical link between rows $m-1$ and m is broken while all the others are connected. Also, all horizontal links on the m 'th row are broken. This corresponds to the case where at step m , a single operator Z_i is measured.
- With probability $\frac{1}{2}(1-p_s)$ all vertical links between rows $m-1$ and m as well as a random horizontal link on row m are connected. All the other horizontal links on the m 'th row are broken. This corresponds to the case where at step m , one of the stabilizer operators is measured.

As can be seen, the vertical links are mostly connected while the horizontal links are mostly broken. However, given that M is equal to $2N^2$ ($2N$ time steps where each time step is consisted of N updating steps), the lattice is elongated along the vertical direction.

As discussed in the main text, the entanglement entropy of the state at step M can be read off entirely from the properties of the percolation lattice.

As is discussed in Section IV the critical exponents ν and z of this percolation model are the same as of the standard link

percolation model on square lattice, thus suggesting it to be in the same universality class. Moreover, even the critical probability p_c is the same. We also find that the coefficients of the entanglement entropy a_x and a_t computed in this model coincide with those of the circuit model defined in Appendix H, which does map exactly to standard percolation on the square lattice.

Appendix E: The duality map

For simplicity, consider the system with periodic boundary conditions. Let us define the Clifford unitary U_d such that for $i = 1, \dots, N$,

$$U_d X_i U_d^\dagger = X_i \quad (\text{E1})$$

$$U_d Z_i U_d^\dagger = X_{i-1} Z_i X_{i+1} \quad (\text{E2})$$

Note that under U_d , the stabilizer g_i transforms as

$$U_d g_i U_d^\dagger = Z_i. \quad (\text{E3})$$

Eq. (E3) and Eq. (E2) together show that the ensemble of random quantum circuits at p_s (and $p_u = 0$) is mapped to the ensemble of random quantum circuit at $1 - p_s$ (and $p_u = 0$) under U_d . However, the unitary U_d is not local, i.e. it cannot be written as the tensor product of on-site unitaries and therefore does not keep the entanglement structure invariant. Nonetheless, it is clear from Eq. (E1) and Eq. (E2) that U_d maps local stabilizers to local stabilizers. Since the entanglement in stabilizer states is related to the number of independent stabilizers that traverse the boundary of a region[31], one can still say that U_d maps a state with the area-law entanglement to an area-law entangled state. Hence, if there exists a continuous phase transition which has logarithmic entanglement scaling, it has to occur at $p_s = p_c = 1/2$. In the following this argument is made rigorous.

Consider the stabilizer state $|\psi\rangle$ specified by the stabilizer set $\mathcal{S} = \{s_1, s_2, \dots, s_N\}$ (see Appendix B for the notation). Let A be the subset of qubits in the segment starting from the qubit q_l and ending with the qubit q_r . Without loss of generality, we assume s_1, \dots, s_m generate the subgroup $\mathcal{G}_{A,\psi}$. Thus,

$$\mathcal{G}_{A,\psi} = \langle s_1, s_2, \dots, s_m \rangle, \quad \log_2 |\mathcal{G}_{A,\psi}| = m. \quad (\text{E4})$$

We can also assume that at most 2 stabilizers from the set $\{s_1, s_2, \dots, s_m\}$ have non-trivial support on q_l because if it is not the case, we can always use two of them to cancel the support of the others on q_l by considering their multiplication with the rest. The same statement holds for q_r as well.

Now consider the state $|\psi'\rangle = U_d |\psi\rangle$ which corresponds to the stabilizer set $\mathcal{S}' = \{U_d s_1 U_d^\dagger, U_d s_2 U_d^\dagger, \dots, U_d s_N U_d^\dagger\}$. Since U_d moves the endpoint of a stabilizer by at most one site, at least $m-4$ out of m stabilizers in $\{U_d s_1 U_d^\dagger, U_d s_2 U_d^\dagger, \dots, U_d s_m U_d^\dagger\}$ are still contained in A , which means $\log_2 |\mathcal{G}_{A,\psi'}| \geq m-4$. Therefore,

$$S_A(U_d |\psi\rangle) \leq S_A(|\psi\rangle) + 4, \quad (\text{E5})$$

which shows that if $|\psi\rangle$ has area-law entanglement, $U_d |\psi\rangle$ should have area-law entanglement as well.

Appendix F: Graphical representation of the state

In this section we develop a graphical description to follow the system's state as it evolves under the random quantum circuit described in Section II for $p_u = 0$. Moreover, this graphical representation provides the basic intuition behind the percolation mapping.

The initial state of the system is given by the stabilizer set $\mathcal{S}_0 = \{Z_1, Z_2, \dots, Z_N\}$. At each step of the circuit, we measure either a stabilizer g_i or a single qubit operator Z_i on a qubit and update the stabilizer set accordingly. Let \mathcal{S}_m denote the stabilizer set that corresponds to the system's state after m updating steps.

First, we prove the following Lemma:

Lemma 2. \mathcal{S}_m can be chosen such that each of its elements, up to a minus sign, is in one of the following forms:

$$\begin{aligned} Z_{2j+1,2k+1} &\equiv \prod_{i=j}^k Z_{2i+1}, \\ Z_{2j,2k} &\equiv \prod_{i=j}^k Z_{2i}, \\ g_{2j+1,2k+1} &\equiv \prod_{i=j+1}^k g_{2i} = X_{2j+1} Z_{2j+2,2k} X_{2k+1}, \\ g_{2j,2k} &\equiv \prod_{i=j}^{k-1} g_{2i+1} = X_{2j} Z_{2j+1,2k-1} X_{2k}, \end{aligned} \quad (\text{F1})$$

for some integers j and k .

Proof. We prove the lemma by induction. The claim is clearly true for \mathcal{S}_0 . Assume it is true for \mathcal{S}_m . First consider the case where we measure Z_{2j+1} in the next step. We follow the procedure proscribed by the Gottesman-Knill theorem [33, 34] to obtain the stabilizer set \mathcal{S}_{m+1} . If Z_{2j+1} commutes with every stabilizer in \mathcal{S}_m , then nothing happens by measuring Z_{2j+1} , hence $\mathcal{S}_{m+1} = \mathcal{S}_m$. So consider the case where some elements of \mathcal{S}_m anti-commute with Z_{2j+1} .

Any element of \mathcal{S}_m that does not commute with Z_{2j+1} has either the form $g_{2j+1,2k+1}$ or $g_{2k+1,2j+1}$ for some k . If there is only one of them, then one only needs to replace it with $\pm Z_{2j+1}$ (with the sign chosen arbitrarily) to obtain \mathcal{S}_{m+1} . If there are more than one, we replace the first one with $\pm Z_{2j+1}$, again with the sign chosen arbitrarily, and multiply the others with the stabilizer that was replaced, to get \mathcal{S}_{m+1} . In either cases, \mathcal{S}_{m+1} will have the stated form.

The other possibilities, i.e. measuring other operators at step $m+1$, can be treated similarly. \square

Based on Lemma 2, we can use a diagrammatic notation to specify \mathcal{S}_m ; we put N dots along a line representing the qubits, as is shown in Fig. 6. Then, for every $g_{a,b}$ element in \mathcal{S}_m , we draw a line between sites a, b from below and for every $Z_{a,b}$ element in \mathcal{S}_m draw a line from above. Fig. 6a and Fig. 6b show the diagrams corresponding to $\mathcal{S} = \{Z_i\}_{i=1}^N$ and $\mathcal{S} = \{g_i\}_{i=1}^N$ respectively, with g_1 and g_N defined as $g_1 \equiv G_1$ and $g_N \equiv G_2$.

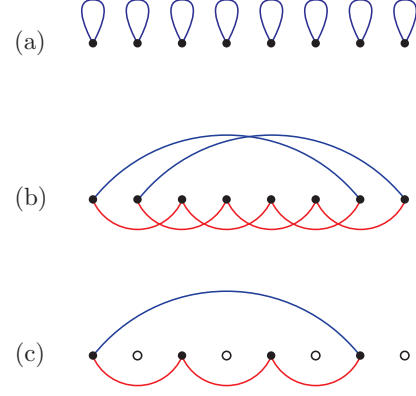


FIG. 6. (a) The diagrammatic representation of the product state $|0\rangle^N$. (b) The diagrammatic representation of the stabilizer state specified by $\mathcal{S} = \{g_i\}_{i=1}^N$. (c) the same as (b) but including just the odd sites.

The form of the stabilizers listed in Lemma 2 suggests a decomposition of the system into odd and even sites. Note that if we measure, for example, Z_{2i+1} , the only stabilizers that could be replaced are in the form $g_{2j+1,2k+1}$ while the $g_{2j,2k}$ stabilizers whose endpoints reside on even sites remain unchanged. Also, if one measures $g_{2i-1,2i+1} = g_{2i}$ whose endpoints are on odd sites, the only stabilizers that could change have the form $Z_{2j+1,2k+1}$. So, if the stabilizer we are measuring has endpoints on odd sites, we only need to know about the stabilizers in \mathcal{S}_m which also end on odd sites to find \mathcal{S}_{m+1} . In other words, we can keep track of the set of stabilizers that start and end on odd sites, without knowing anything about the other stabilizers which start and end on the even sites and vice versa. This allows us to consider odd sites and even sites separately. Fig. 6c shows the same state as in Fig. 6b but restricted to odd sites only. For simplicity, we will only consider odd sites in what follows, while similar statements hold for even sites as well.

Using this diagrammatic formalism, it is easy to track \mathcal{S}_m . Fig. 7 shows a typical quantum circuit and the step by step evolution of the system's stabilizer set using the diagrammatic notation developed above.

Appendix G: Proof of Proposition 1

We start by noting that for the circuit shown in Fig. 7, the state of the system can always be described as a collection of isolated SPT states and decoupled qubits, as can be seen from the accompanying diagrammatic representation. For example, in the final state, qubits 1, 5 and 7 form an isolated SPT state, while qubit 3 is decoupled. This observation is indeed true in general. We start by putting forward a precise definition of an isolated SPT state and then show that there is an efficient description of \mathcal{S}_m as a partition of $\{1, 2, \dots, N\}$.

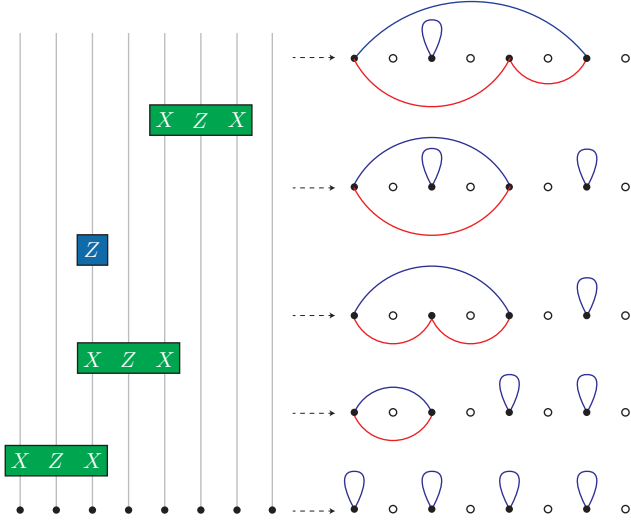


FIG. 7. Step by step evolution of the system under the quantum circuit shown on the left. The diagrammatic representation of the system's state is shown on the right after each measurement.

Definition 1. Consider a set of numbers $A = \{q_i\}_{i=1}^n$, such that,

$$1 \leq q_1 < q_2 < \dots < q_n \leq N. \quad (\text{G1})$$

Assume that all numbers are either odd or even. Define its associated stabilizer set, denoted by $\mathcal{S}(A)$, as

$$\mathcal{S}(A) = \{g_{q_i, q_{i+1}}\}_{i=1}^{n-1} \cup \left\{ \prod_{i=1}^n Z_{q_i} \right\}. \quad (\text{G2})$$

We call such a stabilizer set, an isolated SPT state.

Note that the g stabilizers in $\mathcal{S}(A)$ generate the set of all g strings between any two points in A . Also, note that the stabilizers in Eq. (G2) are the same as the ones appearing in Proposition 1.

Lemma 3. Let \mathcal{S}_m denote the stabilizer set that corresponds to the system's state after m updating steps. \mathcal{S}_m can always be chosen such that, up to minus signs,

$$\mathcal{S}_m = \cup_i \mathcal{S}(A_i), \quad (\text{G3})$$

where A_i s correspond to a partition of the qubits into disjoint sets,

$$\cup_i A_i = \{1, 2, \dots, N\}. \quad (\text{G4})$$

and $\mathcal{S}(A_i)$ denotes the isolated SPT state corresponding to subset A_i .

Proof. We prove it by induction. It is obviously true for \mathcal{S}_0 with $A_i = \{i\}$ for $i = 1, \dots, N$.

Now assume it is true for \mathcal{S}_m , so there exists a partition of qubits given by $\{1, 2, \dots, N\} = \cup_i A_i$ such that $\mathcal{S}_m =$

$\cup_i \mathcal{S}(A_i)$. First consider the case in which a single qubit operator Z_{2j+1} is measured in the next step. Suppose $2j+1$ is in subset A_k for some k . Note that Z_{2j+1} commutes with any element in $\mathcal{S}(A_{k'})$ with $k' \neq k$. If A_k is the single element set $\{2j+1\}$ (which means $\mathcal{S}(A_k) = \{Z_{2j+1}\}$) then Z_{2j+1} is already in \mathcal{S}_m and thus $\mathcal{S}_{m+1} = \mathcal{S}_m$. If A_k has more than one element, we will show that measuring Z_{2j+1} corresponds to breaking A_k to two subsets of $A_k \setminus \{2j+1\}$ and $\{2j+1\}$.

Note that Z_{2j+1} anti-commutes only with the $g_{a,b}$ elements in $\mathcal{S}(A_k)$ where either a or b equals $2j+1$. If $2j+1$ is the smallest or largest number in A_k , there is only one such element and by measuring Z_{2j+1} , we just need to replace that element by Z_{2j+1} (with an arbitrary sign) to get the updated stabilizer set \mathcal{S}_{m+1} . If $2j+1$ is neither the smallest nor the largest number in A_k , there are two such elements, $g_{a,2j+1}$ and $g_{2j+1,b}$ for some odd numbers a and b . Thus by measuring Z_{2j+1} , one is replaced by Z_{2j+1} (with an arbitrary sign) and the other by $g_{a,2j+1}g_{2j+1,b} = g_{a,b}$ to get the updated stabilizer set. It is easy to verify that in both cases, \mathcal{S}_{m+1} is equivalent to the stabilizer set obtained by the union of isolated SPT states corresponding to the same partitioning as for \mathcal{S}_m , but with A_k broken to two sets of $A_k \setminus \{2j+1\}$ and $\{2j+1\}$.

Next consider the case where an stabilizer $g_{2j-1,2j+1} = g_{2j}$ is measured in the next step. If $2j-1$ and $2j+1$ belong to the same subset in the partition, nothing happens. If not, let say one belongs to A_k and the other to $A_{k'}$, then $g_{2j-1,2j+1}$ anti-commute with the two Z chains in $\mathcal{S}(A_k)$ and $\mathcal{S}(A_{k'})$ and commutes with everything else in \mathcal{S}_m . Therefore, by measuring $g_{2j-1,2j+1}$, we replace one of the Z chains with $\pm g_{2j-1,2j+1}$ (with an arbitrary sign) and the other with the product of the two Z chains, which is just the Z chain over $A_k \cup A_{k'}$, to get \mathcal{S}_{m+1} . It is straightforward to verify that \mathcal{S}_{m+1} is equivalent to the stabilizer set obtained by union of isolated SPT states corresponding to the same partitioning as for \mathcal{S}_m , but by merging the two subsets A_k and $A_{k'}$ into a single subset $A_k \cup A_{k'}$. \square

Based on Lemma 3, there is a one-to-one mapping between partitions of $\{1, 2, \dots, N\}$ and the state of the system. Moreover, as can be seen from the Lemma's proof, the dynamics of the system can be translated into merging and splitting of the subsets.

Let us specify a partition by assigning unique colors to the qubits in the same subset. Then, whenever a Z operator is measured, a new unique color should be assigned to the corresponding qubit to account for the new single element subset that is created in the new partitioning. On the other hand, when a g operator with end points in different subsets is measured, the two subsets merge together which translates into assigning the same color to qubits in either one. The dynamics we have just described emerges naturally in the percolation model and thus can be used to map the quantum circuit to an instance of percolation on the square lattice. We use a $N/2 \times M$ square lattice, where M is the total number of updating steps. The m 'th row of the lattice corresponds to the state of the system after the updating step m . We start by $N/2$ dots with distinct colors at the lowest row which corresponds

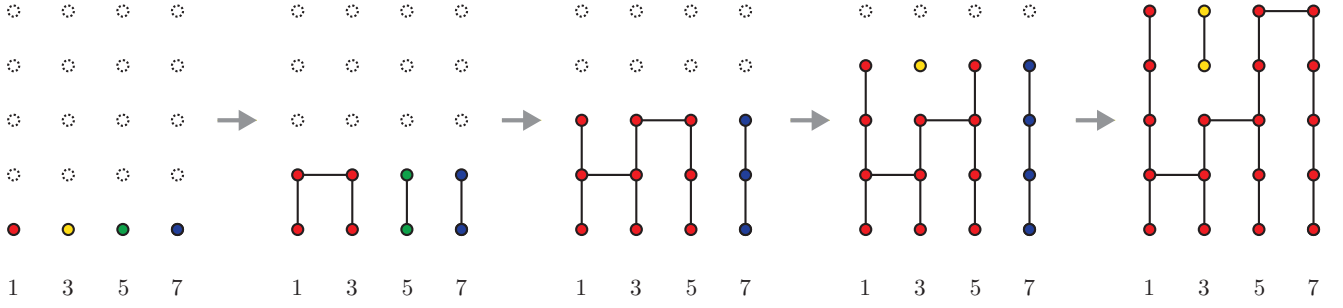


FIG. 8. Step by step evolution of the system under the quantum circuit shown in Fig. 7 in the percolation picture for the odd sites. At each step, the sites with the same color on the last row represent an isolated SPT phase. There is an analogous diagram for the even sites. The two diagrams together fully specify the entanglement structure of the system.

to the initial product state. If Z_{2i+1} is measured at step m , we leave the vertical link between $(2i+1, m)$ vertex and its history at $(2i+1, m-1)$ broken, while connecting all the other vertical links between the rows m and $m-1$. By doing so, the $(2i+1, m)$ vertex gets a new color, while all the other vertices retain their color from the previous row, which agrees with the aforementioned splitting. On the other hand, if a stabilizer $g_{2i-1, 2i+1}$ is measured at step m , we first connect all the vertical links between the rows m and $m+1$, and then connect the vertices at $(2i-1, m)$ and $(2i+1, m)$ to enforce their colors to be the same, thus accounting for the aforementioned merging. Therefore, in each step, the colors of the last updated row can be used to find the partitioning of qubits mentioned in Lemma 3, which completes the proof of Proposition 1.

As an example, Fig. 8 shows the step by step development of the circuit described in Fig. 7, in the percolation picture.

It is worth noting that the stabilizer set given in Lemma 3 is already in the clipped gauge (see Appendix B for the definition of clipped gauge). Therefore, the entanglement structure can be inferred readily from the percolation picture. In particular, the entanglement entropy $S(x)$ of the region $[1, x]$, is equal to the number of clusters with support on both inside and outside of the region $[1, x]$ on the top row of the percolation lattices.

Appendix H: Random measurement circuit corresponding to standard percolation

Here we present a slightly different random circuit model than the one presented in the main text, which maps to the standard bond percolation on a square lattice. We define this circuit model using only the competing single qubit and stabilizer measurements, without including any unitary dynamics.

The random circuit model has a layered configuration of measurements, as follows. At alternating layers, we measure either only stabilizer operators or only single qubit operators, as shown in Fig. 9. Two consecutive layers of measurements

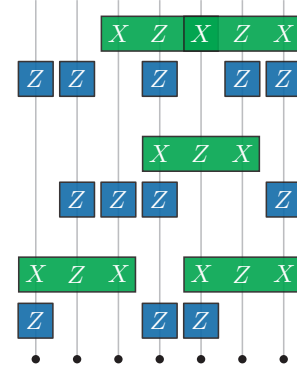


FIG. 9. The random circuit which maps to the standard bond percolation on a square lattice. On the last layer of the figure, two stabilizers which have overlap are measured. Since the stabilizers commute with each other, the order of the measurements does not matter.

correspond to a time step (here, there is no distinction between updating steps and time steps). In the layer where stabilizers are measured, for each i we measure g_i with probability p_t . In the layer where the single qubit operators are measured, for each i we measure Z_i with probability $1 - p_t$. Fig. 9 shows a typical realization of the circuit. Note that it is possible for two stabilizer measurements in the circuit to overlap with each other, but since the corresponding operators commute with each other, they can still be measured simultaneously.

Note that the percolation mapping described in Appendix G is based on the specific form of the measurements involved rather than their layout on the circuit. Since the exact same set of measurements are involved in the quantum circuit described here, one can use the same rules, as is explained in Section II, to map this circuit model to two percolation models on square lattices. It is easy to verify each of the corresponding percolation models is indeed the standard bond percolation on an $N \times 2N$ square lattice where each bond

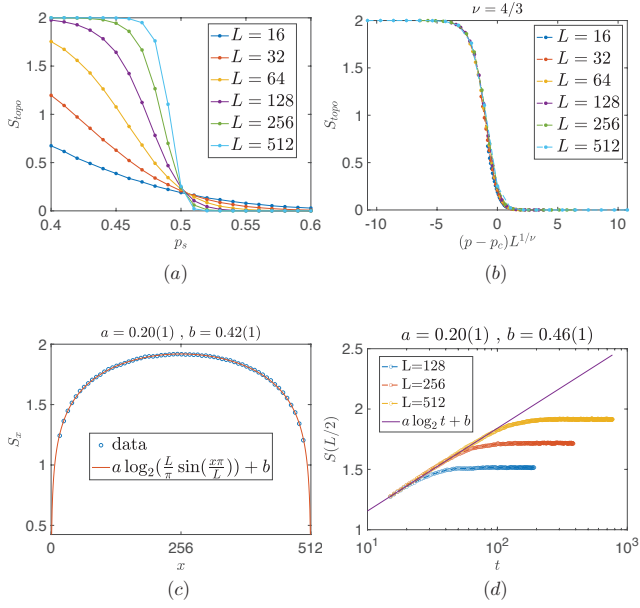


FIG. 10. Entanglement plots for the circuit with layered configuration. (a) Topological entanglement entropy S_{topo} versus single qubit measurement probability which shows the same phase transition at $p_c = 0.5$. (b) Scaling collapse of the data in (a) for $\nu = 4/3$ using the same scaling as in Eq.(9). (c) The entanglement entropy of the $[0, x]$ segment of the chain in the steady state at $p = p_c$ and $L = 512$. (d) The entanglement entropy of the half-chain versus time for $p_s = p_c$.

is connected with probability p_t . We focus on the odd sites' lattice, for example, and include a horizontal bond with probability p_t , corresponding to a stabilizer measurement. A vertical bond is included with probability p_t , corresponding to the absence of a single qubit measurement.

Fig. 10 is analogous to Fig. 3, but for the random circuit model with the layered structure. The phase transition happens at $p_c = 1/2$ and the critical exponent is found to be $\nu = 4/3$, as is expected from the percolation mapping. We also find $a_x = a_t = 0.20(1)$, the same values as the ones in the original circuit model in the main text.

Appendix I: Supplemental Figures

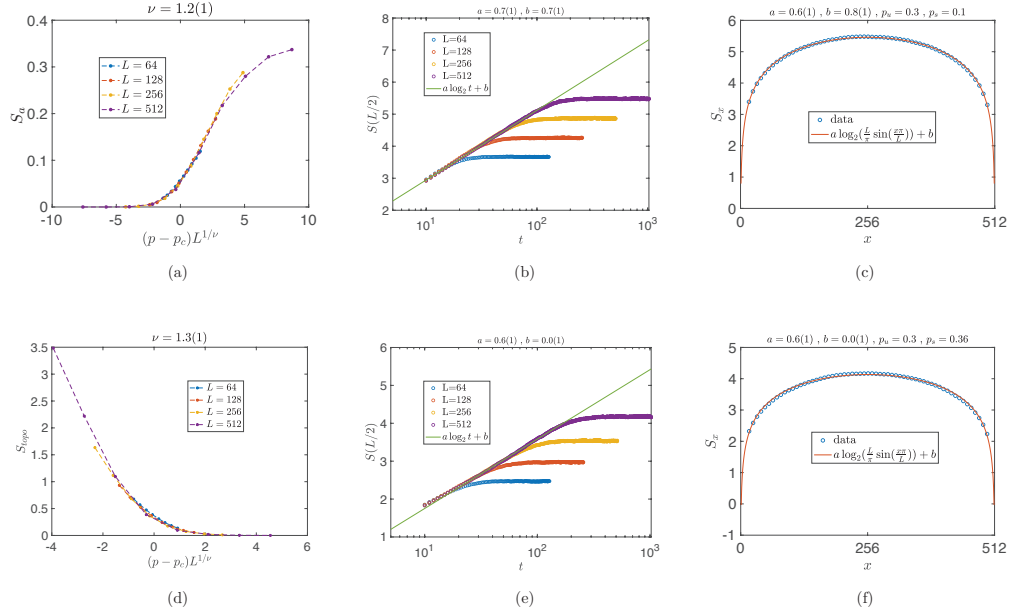


FIG. 11. Additional plots for the two phase transitions along the line $p_u = 0.3$. The first row corresponds to the data for the SPT to volume law phase transition at $p_s = 0.10(1)$ and the second row corresponds to the data for the volume law to trivial phase transition at $p_s = 0.36(1)$.

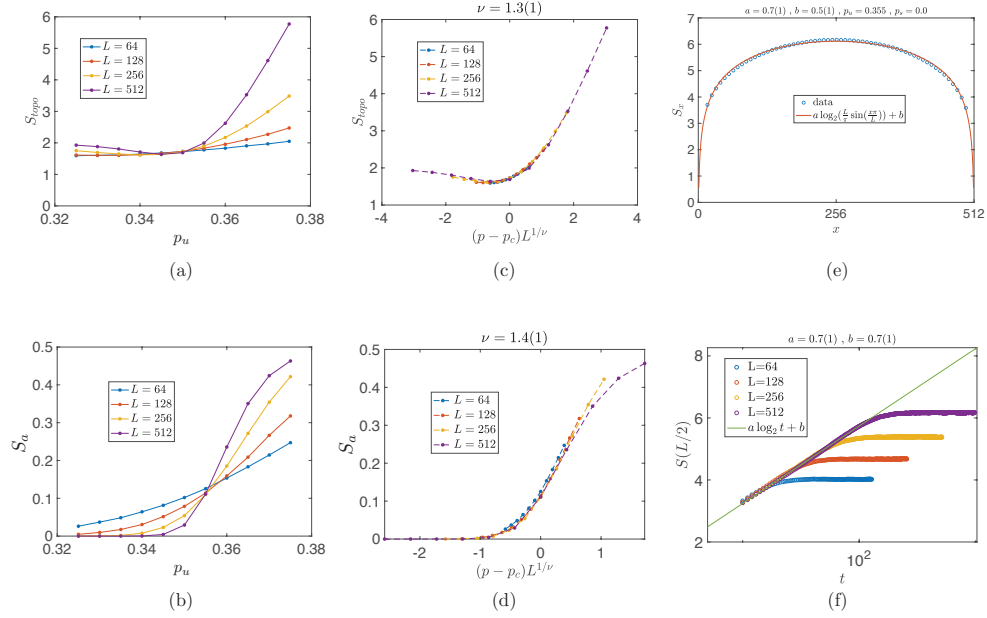


FIG. 12. Plots corresponding to the critical point on the p_u axis, with $p_s = 0$. As can be seen from (a) and (b), the phase transition occurs at $p_u = 0.355(5)$.

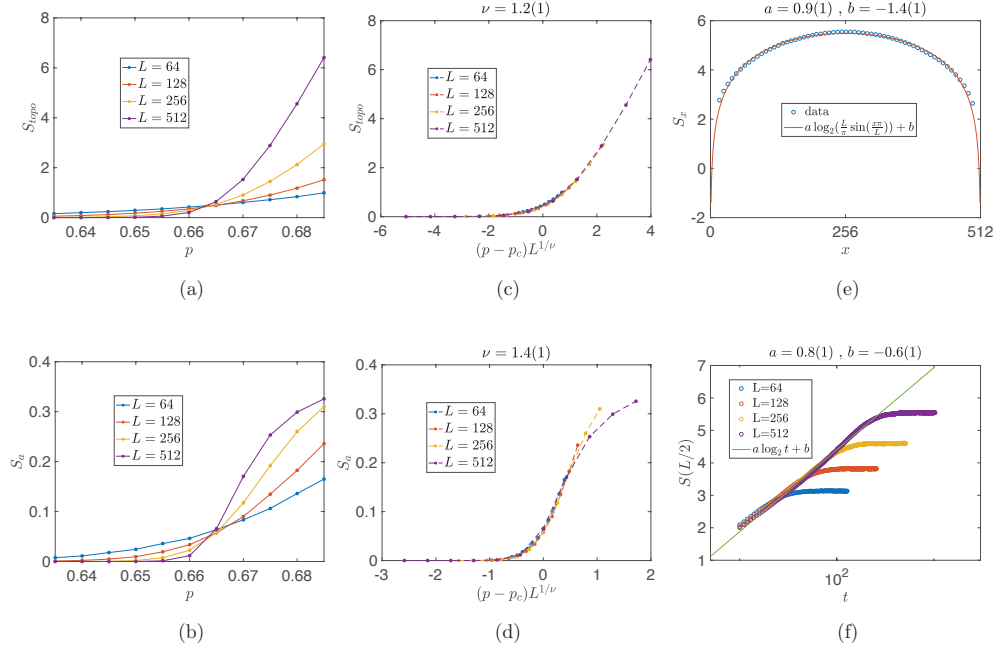


FIG. 13. Plots corresponding to the critical point on the $p_u + p_s = 1$ line. As can be seen from (a) and (b), the phase transition occurs at $p_u = 0.665(5)$ and $p_s = 1 - p_u = 0.335(5)$.